Global modes of climate variability

O. de Viron,[1] J. O. Dickey,[2] M. Ghil,[3]

[1]Université Paris Diderot, Sorbonne Paris Cité, and Institut de Physique du Globe de Paris (UMR7159)

[2]Jet Propulsion Laboratory, California Institute of Technology, Pasadena, CA

[3]Ecole Normale Supérieure, Paris, and University of California, Los Angeles, USA

This article has been accepted for publication and undergone full peer review but has not been through the copyediting, typesetting, pagination and proofreading process, which may lead to differences between this version and the Version of Record. Please cite this article as doi: 10.1002/grl.50386

The atmosphere, hydrosphere and cryosphere form a fully coupled climate system. This system exhibits a number of large-scale phenomena, such as the El Niño–Southern Oscillation (ENSO), the Asian Monsoon, the North Atlantic Oscillation (NAO), and the Madden-Julian Oscillation (MJO). While these modes of variability are not exactly periodic, they are oscillatory in character, and their state is monitored using so-called climate indices. Each of these scalar indices is a combination of several climate variables. Here, we use a comprehensive set of 25 climate indices for time intervals that range between 1948 and 2011, and estimate an optimal set of lags between these indices to maximize their correlation. We show that most of the index pairs drawn from this set present a significant correlation on interannual time scales. It is also shown that, on average, about two-thirds of the total variability in each index can be described by using only the four leading principal components of the entire set of lagged indices. Our index set's leading orthogonal modes exhibit several interannual frequencies and capture separately variability associated with the North Atlantic and the North Pacific. These modes are associated, in turn, with large-scale variations of sea surface temperatures.

1. Introduction

The Earth's atmosphere, oceans, cryosphere, and continental hydrology exchange mass, momentum and energy on all time scales. As a consequence, global- or regional-scale climate variables — such as the sea surface temperature (SST), the rainfall, the surface pressure or the wind speed — fluctuate more or less regularly. Many of these fluctuations are known as modes or oscillations, and their states are monitored by using scalar-valued climate indices. Some of the best-known oscillations extend over large areas of the globe; they include ENSO, the NAO, the Pacific Decadal Oscillation (PDO) and the MJO. Certain oscillations are more localized, i.e. associated with the climate of smaller regions, e.g., the Sahel Rainfall; however, many teleconnections [*Wallace and Gutzler*, 1981] between the latter indices are also known to exist.

Numerous authors have studied such teleconnections and the, possibly lagged, correlations between up to four indices [*Ambaum et al.*, 2001; *Moonley and Munot*, 1993; *Tsonis et al.*, 2007; *Wyatt et al.*, 2011; *Wang et al.*, 2012]. Other studies have considered the dynamics of coupled nonlinear oscillators as a possible source for such correlations [*Ghil and Mo*, 1991; *Kimoto and Ghil*, 1993; *Feliks et al.*, 2010] or studied the network of time series of a single climate field, such as the SSTs, at the nodes of a regular grid [*Tsonis and Swanson*, 2008; *Donges et al.*, 2009].

In this study, we investigate whether and to which extent a large set of climate indices — which presumably capture the coupled dynamics of several climate fields — may exhibit lagged correlations on a global scale and, if so, what possible causes such a phenomenon may have.

In Section 2, we describe the data used, and how they were preprocessed. In Section 3, we investigate the connections between the climate indices. Section 4 makes the link between our results and variations of the the SST field. The spectral content of the retrieved modes is discussed in Section 5. Concluding remarks follow in Section 6.

2. Data Sets and Their Preparation

For this investigation, we use a set of 25 climate indices, regional as well as global; their complete list — with acronyms, time intervals of availability and source — is given in Table 1.

This set of time series consists of the entire set of climate indices from NOAA's Earth System Research Laboratory, with four exceptions: (i) only the Southern Oscillation Index (SOI) has been kept among the different ENSO-related time series, since all of these are highly correlated with each other, and their inclusion would have led to climatically superfluous numerical difficulties; (ii) the atmospheric angular momentum has been removed, since previous studies showed that its interannual variability was linked to ENSO [*Stefanick*, 1982]; and (iii) the solar constant variability was dropped, as it is not a climatic index *per se*. Finally, (iv) the MJO index was added to the set because its interannual modulation is a topic of particular interest to the authors (e.g., *Marcus et al.* [2001]).

To separate the interannual contribution, we started by removing a composite seasonal cycle, i.e. the average value over all the months of January in the time series has been subtracted from each January value, and so on. The linear trend of each time series was then fitted and removed. Finally, a tapered low-pass filter with a cut-off frequency of 12 months has been applied by convolution of the time series with $\sin(2\pi f t)/(2\pi f t)$, where

f is the cut-off frequency [*Owen*, 2007]. The resulting time series for each index has been divided by its own standard deviation, in order to normalize the different indices with respect to each other.

In Section 5, we used the global SST fields of *Kaplan et al.* [1998].These SSTs have monthly resolution and are given on a 2.5°x2.5° grid.

3. Connections Between Climate Indices

3.1. Cross-correlations

In order to study the connections between the indices, we start by cross-correlating pairs of indices, up to a maximum lag of one year. The correlation coefficient used in this study is the Pearson product-moment coefficient. Cross-correlations are computed by shifting one time series by a given number of months with respect to the other.

We first computed cross-correlations for lags between $+1$ year and -1 year, in steps of 1 month, and then computed the significance for the lag with the highest cross-correlation. The significance is computed using a Student t-test, after estimating the number of degrees of freedom of the time series, cf. *Von Storch and Zwiers* [1999].

The number of degrees of freedom was estimated for each pair of time series as the harmonic mean of the number of degrees of freedom from the two time series over the common time interval; this number was computed for each of the two series as the ratio between the common time interval and the decorrelation time of the series in question, i.e. the lag at which its autocorrelation drops to $1/e$.

Figure 1 summarizes the cross-correlation results. For each index pair, a colored square indicates the maximum value of the cross-correlation for those pairs of indices for which the statistical significance exceeds 95%; all other correlations appear as white squares. The figure shows that more than 60% of the pairs are significantly cross-correlated.

3.2. Principal components (PCs) and optimization procedure

To investigate the common content in our set of time series $\{x_i(t) : i = 1, ..., n\}$, we apply principal component (PC) analysis [*Von Storch and Zwiers*, 1999], and project them onto the eigenvectors of their variance-covariance matrix. This way, the set of 25 climate indices is expressed as a linear combination of the eigenvectors $\{X_k(t) : k = 1, \ldots, K\}, K \leq n = 25$, which are orthogonal at zero lag,

$$x_i(t) = \sum_{k=1}^{K} a_{i,k} X_k(t).$$

When several time series are interrelated, much of the variance is associated with only a few PCs, $K \ll n$. As we want to allow lags between the different indices, we used a slightly different version of PC analysis, and optimized a set of lags between the indices so that the variance captured by four PCs is maximized. The choice of $K = 4$ PCs was based on Monte-Carlo tests [*Overland and Preisendorfer*, 1982], which showed that the first four PCs are significant, and that adding a few more does not modify the picture in any substantial way.

Given the relatively large dimension of the set of climate indices and, a fortiori, of the set of possible lags between them, we started with a random set of lags, and used a genetic algorithm [*Goldberg*, 1989] to converge to the optimal set. Since the intervals of availability of the 25 indices differ, we used 126 different time intervals, including in each of them only the indices available in that interval. The 126 intervals correspond to 14 starting times, from 1955 to 1981 by steps of 2 yr, and nine ending times, from 1995 to 2011 by steps of 2 yr; the interval lengths thus range from 15 to 55 yr, with a median value of 35 yr. The optimal set of lags was computed for each time interval.

If a connection between two indices does exist, the difference between the lags of those indices — with respect to an arbitrary origin — would be consistent over the 126 runs, whereas the absence of a robust connection between the two would manifest itself as a random distribution of the difference between their lags. We tested each lag-difference distribution against a uniform distribution by using a χ^2-test and found that the distributions so tested were significantly distinct from random (at the 95% level) for about 60% of the pairs of indices. Altogether, more than 80% of the index pairs have either a cross-correlation that is significant at the 95% level or a robust lag, or both.

Next, an overall least-square fit was performed in order to find a globally optimal set of lags, based on the best lags found between pairs of modes over all the runs. We also estimated a weighted solution, in which each run is weighted according to the variance captured by the first four modes; both solutions are provided in Table 1. The difference between the weighted and unweighted lags only exceeds one full month in three cases, all of which represent relatively local phenomena, and it is larger than one full year in only one of these three. We then used these optimized lags to compute four PCs over the subset of indices that are defined over the entire interval, $1955 - 2011$.

Each of the indices was then reconstructed as a linear combination of the four PCs over its own interval of availability, and we computed for each of them the variance so described. The contribution of each of the four PCs to each of the 25 modes, and the total variance captured in each case, are shown in Figure 2. It is clear from the figure that the variance described by a linear combination of the four PCs is below 50% for only six of the 25 indices. It also allows one to group the indices dominated by the same PC.

The group associated with the first PC (red bars) includes mostly Atlantic-related indices — the Atlantic Multidecadal Oscillation (AMO), the Tropical North Atlantic mode, the Atlantic Meridional Mode, Caribbean SSTs and the Atlantic Tripole — along with a few other indices, such as the global mean SST and the Western Hemisphere warm pool. Some of these links, like the one between the AMO and the Tropical North Atlantic mode, have been recognized in previous studies [*Trenberth and Shea*, 2006]. The AMO involves the buoyancy-driven meridional overturning of the entire Atlantic Ocean [*Delworth et al.*, 1993; *Chen and Ghil*, 1996] and it does seem to have a near-global climate impact [*Knight et al.*, 2006; *Wang et al.*, 2008].

The group of indices that is associated with the second PC (blue bars) appears to be linked with the Pacific Ocean. This PC captures much of the PDO, ENSO, the Tropical Pacific SST pattern, the Northern Oscillation and the North Pacific pattern, with smaller contributions to other modes, such as the MJO, the Antarctic Oscillation and the NAO. *Pohl et al.* [2010] already documented a connection between ENSO, the Antarctic Oscillation and the MJO, and so did *Giannini et al.* [2001] for ENSO and the NAO. The near-global effects of ENSO have, of course, been a matter of intensive study over the last three decades[*Philander*, 1990; *Sarachik and Cane*, 2010].

The third PC (green bars) is associated mostly with the Arctic Oscillation, the NAO, and the Tropical Southern Atlantic index. Links between the Arctic Oscillation and the NAO have also been studied, but are known to exhibit various complexities in their details [*Ambaum et al.*, 2001; *Kravtsov et al.*, 2006]. The last PC is associated with smaller contributions to the variance of a few tropical and Atlantic indices.

4. Teleconnections and the SST Field

In studying the dynamics of the climate system on interannual and longer time scales, it is natural to investigate the role of the oceans and of their variability [*National Research Council*, 1995]. Consequently, we computed a lag correlation between the global SST field [*Kaplan et al.*, 1998] and our four leading PCs. In Figure 3, we show a map of the lagged cross-covariances between the SST field and each of the four PCs, at the lag that maximizes the sum of the absolute values of the correlations over the whole map. The cross-covariance has been set to zero, and thus appears in white on the respective map, wherever the cross-correlation is not significant at the 95% level.

As expected for global-scale phenomena, the cross-covariances are quite substantial over large areas of the World Ocean. The SST pattern correlated with the first PC is consistent with the SST signature of the AMO [*Messié and Chavez*, 2011], and the second one with the classical pattern of the PDO [*Weare et al.*, 1976; *Mantua et al.*, 1997; *Chao et al.*, 2000]. The cross-covariances in Fig. 3(a) are largest in the North Atlantic's subpolar seas, off Japan, and in several marginal seas, including the Mediterranean and the Baltic.

The SST field is lagging here by roughly one year, while it is leading by about one year in the other three panels. Note that the time origin of the PCs is arbitrary, as it is based on a lagged set of indices; hence only the relative lags are meaningful.

In Fig. 3(b), the cross-covariances are largest in the Kuroshio extension and, with the opposite sign, along parts of the West Coast of North America, in good agreement with the dominance of the PDO for this PC. For the third PC, however, the cross-covariances are not particularly consistent with the Arctic Oscillation. This lack of consistency may be due, at least in part, to the complex relationships between the Arctic Oscillation and the NAO [*Ambaum et al.*, 2001; *Kravtsov et al.*, 2006]. The cross-covariances here are largest in the South Pacific Convergence Zone and off the West Coast of Africa; the latter region is dominated by the Benguela Current and prominent also in Fig. 3(a). Finally, in Fig. 3(d), the area of significant cross-covariances is much smaller than in the first three panels, being essentially restricted to to the Tropical Pacific, the California Current, and the Carribbean.

5. Spectral Content

Finally, we inquired into the extent to which more or less regular behavior in time might be associated with the four leading modes. First, each PC was analyzed using the MTM method, without pre-filtering. We found peaks at periods close to 2.5 yr and 3.5 yr for all the PCs, 5.7 yr for mode 3, and 4.3 yr for PCs 2 and 3; see Table 2, right column. The peaks were tested using a median-filter robustness test [*Mann and Lees*, 1996]. Various taper numbers n, with $5 \le n \le 10$, and the corresponding resolution parameters p, with $p = 2n - 1$, were tested, without any noticeable change of the results.

Each PC was then analyzed using singular spectrum analysis (SSA), cf. *Ghil et al.* [2002] and references therein. The SSA decomposition was performed iteratively: an embedding window M is chosen in order to optimize the frequency concentration of the first mode, i.e. of the first pair of eigenvectors associated with nearly equal variances; the associated reconstructed component is then subtracted, and the residual is analyzed the same way, until eight modes or pairs have been estimated. The embedding window M is chosen large for the first SSA run, in order to capture the long-periodic behavior, whereas we use $M \approx 140$ months, i.e., roughly 12 yr, for the next runs.

The maximum-entropy method (MEM) spectrum has been computed both on the sum of the eight SSA modes (see results in Table 2), and on each mode separately. In the first case, a long-term component, with a period longer than 20 yr, and a periodic term around 2.5 yr were identified for each PC; in addition, a 4.5 yr component was found in PC2 and a 5.3 yr component in PC3. Analyzing the modes separately allowed us to confirm the results obtained on the sum of the eight modes, and to detect periodic components of lesser amplitude or longer period: 3.5 yr and 10 yr for PC1; 3.5 yr and 8.5 yr for PC2; 3.6 yr and 10 yr for PC3; 3.2 yr and 10 yr for PC4. These results are robust when changing the MEM order within a reasonable range.

The shorter periods of 3.2–3.6 yr were confirmed by the MTM analysis in each of the four PCs. While not present in the MTM analysis with a high significance, it is of some interest to find the 10-yr peak present in all four PCs, when analyzing the modes separately.

Table 2 summarizes the results from these analyses. All four PCs have a highly significant peak, obtained by both methods, in the range of 2.3–2.8 yr, which is most likely associated with the global effects of ENSO's quasi-biennial oscillation [*Philander*, 1990; *Sarachik and Cane*, 2010; *Ghil et al.*, 2002]. In addition, modes 2 and 3 also exhibit a longer and likewise highly significant period, at 4.3–5.7 yr. This peak might, in turn, be associated with the quasi-quadrennial periodicity of ENSO, modified maybe by the effects of the NAO's 7–8-yr periodicity [*Ghil et al.*, 2002; *Feliks et al.*, 2010]. A longer period, of 21 yr or even longer, is present only in the SSA analysis of all four modes; it could be due to the 17–21-yr period in the PDO [*Chao et al.*, 2000; *Ghil et al.*, 2002], but cannot be significant in our data set, whose length barely exceeds twice the period under consideration.

6. Conclusions

We have thus shown here that 25 different climate indices — associated with a great variety of climatic fields and geographic regions — share a very substantial fraction of their variability. This common fraction can be captured and described by using no more than four leading modes of variability. Much of this variability, in turn, is correlated with the SST field. The preferred periodicities apparent in these modes reflect mainly the quasi-biennial and quasi-quadrennial periodicities of ENSO. The short records, of not much more than 50–60 years, do not allow one to determine unequivocally the longer periods of 7–8 yr of the NAO or the 17–21 yr of the PDO, but some trace of such periodicities is also apparent in our analysis.

Acknowledgments. This study was supported by the U.S. National Science Foundation and the Office of Naval Research (MG), and by the Institut Universitaire de France and the Centre National des Etudes Spatiales through the TOSCA program (OdV). The work of JOD is a phase of research carried out at the Jet Propulsion Laboratory, California Institute of Technology, sponsored by the National Aeronautics and Space Administration (NASA). All but the MJO index time series were provided through the Earth System Research Laboratory web site at http://www.esrl.noaa.gov/psd/data/climateindices/list/. The MJO index time series comes from KNMI's Climate Explorer web site http://climexp.knmi.nl. It is a pleasure to thank the editor (Noah Diffenbaugh) and two anonymous reviewers for their help in improving the paper.

References

Ambaum, M.H.P., B.J. Hoskins, and D.B. Stephenson (2001), Arctic Oscillation or North Atlantic Oscillation? *J. Climate*, *14*(16), 3495–3507.

Chao, Y., M. Ghil, and J.C. McWilliams (2000), Pacific interdecadal variability in this century's sea surface temperatures, *Geophys. Res. Lett.*, *27*, 2261–2264.

Chen, F. and M. Ghil (1996), Interdecadal variability in a hybrid coupled ocean-atmosphere model, *J. Phys. Oceanogr.*, *26*, 1561–1578.

Delworth, T., S. Manabe, and R.J. Stouffer (1993), Interdecadal variations of the thermohaline circulation in a coupled ocean-atmosphere model. *J. Climate*, *6*, 1993–2011.

Donges, J.F., Y. Zou, N. Marwan, J. Kurths (2009), The backbone of the climate network, *Euro. Phys. Lett.*, *87*(4), 48007.

Feliks, Y., M. Ghil, and A.W. Robertson (2010), Oscillatory climate modes in the Eastern Mediterranean and their synchronization with the North Atlantic Oscillation, *J. Climate*, *23*, 4060–4079, doi:10.1175/2010JCLI3181.1.

Ghil, M., and K.-C. Mo (1991), Intraseasonal oscillations in the global atmosphere. Part I: Northern Hemisphere and tropics, *J. Atmos. Sci.*, *48*, 752–779.

Ghil, M., et al. (2002) Advanced spectral methods for climatic time series, *Rev. Geophys., 40*(1), pp. 3.1–3.41, doi: 10.1029/2000RG000092.

Giannini, A., M.A. Cane, and Y. Kushnir, Interdecadal changes in the ENSO teleconnection to the Caribbean region and the North Atlantic Oscillation. *J. Climate*, *14*, 2867-2879 (2001).

Goldberg, D. (1989), *Genetic Algorithms in Search, Optimization, and Machine Learning.* Addison-Wesley.

Kaplan, A., M. Cane, Y. Kushnir, A. Clement, M. Blumenthal, and B. Rajagopalan (1998), Analyses of global sea surface temperature 1856–1991, *J. Geophys. Res., 103*, 18,567-18,589.

Kimoto, M., and M. Ghil (1993), Multiple flow regimes in the Northern Hemisphere winter. Part II: Sectorial regimes and preferred transitions, *J. Atmos. Sci.*, *50*, 2645–2673.

Knight, J.R., C.K. Folland, and A.A. Scaife (2006), Climate impacts of the Atlantic Multidecadal Oscillation, *Geophys. Res. Lett., 33*, L17706, doi:10.1029/2006GL026242.

Kravtsov, S., A.W Robertson, and M. Ghil (2006), Multiple regimes and low-frequency oscillations in the Northern Hemisphere's zonal-mean flow, *J. Atmos. Sci.*, *63*, 840–860.

Marcus, S. L., J. O. Dickey, and O. de Viron (2001), Links between intraseasonal (extended MJO) and ENSO timescales: Insights via geodetic and atmospheric analysis, *Geophys. Res. Lett.,* **28**(18), 3465-3468.

Mann, M.E., and J.M. Lees (1996), Robust estimation of background noise and signal detection in climatic time series. *Clim. Change*, *33*, 409–445.

Mantua, N.J., et al. (1997), A Pacific interdecadal climate oscillation with impacts on salmon production, *Bull. Am. Meteorol. Soc., 78*, 1069–1079.

Messié, M., and F. Chavez (2011), Global modes of sea surface temperature variability in relation to regional climate indices, *J. Climate*, *24*, 4314–4331, doi:10.1175/2011JCLI3941.1.

Moonley, D.A. and A.A. Munot (1993), Variation in the relationship of the Indian Summer Monsoon with global factors. *Proc. Indian Acad. Sci. (Earth Planet. Sci.)*, *102*, 89–104.

National Research Council (1995), *Natural Climate Variability on Decade-to-Century Time Scales*, D. G. Martinson, K. Bryan, M. Ghil et al. (Eds.), National Academy Press, Washington, D.C..

Overland, J.E., and R.W. Preisendorfer (1982), A Significance test for principal components applied to cyclone climatology. *Mon. Wea. Rev.*, *110*, 1–4 .

Owen, M. (2007), *Practical Signal Processing*, Cambridge University Press.

Philander, S.G.H. (1990), *El Niño, La Niña, and the Southern Oscillation*, Academic Press, San Diego.

Pohl, B., N. Fauchereau, C.J.C. Reason, and M. Rouault (2010), Relationships between the Antarctic Oscillation, the Madden-Julian Oscillation, and ENSO, and consequences for rainfall analysis. *J. Climate*, *23*, 238–254.

Sarachik, E.S. and M.A. Cane (2010), *The El Niño-Southern Oscillation Phenomenon*, Cambridge Univ. Press.

Stefanick, M. (1982), Interannual atmospheric angular momentum variability 19631973 and the Southern Oscillation, J. Geophys. Res., 87(C1), 428–432, doi:10.1029/JC087iC01p00428.

Trenberth, K.E., and D.J. Shea (2006), Atlantic hurricanes and natural variability in 2005, *Geophys. Res. Lett., 33*, L12704, doi:10.1029/2006GL026894.

Tsonis, A. A., K. Swanson, and S. Kravtsov (2007), A new dynamical mechanism for major climate shifts, Geophys. Res. Lett., 34, L13705, doi:10.1029/2007GL030288.

Tsonis, A.A. and K.L. Swanson (2008), Topology and predictability of El Niño and La Niña networks, *Phys. Rev. Lett.*, *100*(22), 228502–228506.

Von Storch, H., and F.W. Zwiers (1999), *Statistical Analysis in Climate Research.* Cambridge University Press.

Wallace, J.M., and D.S. Gutzler (1981), Teleconnections in the geopotential height field during the Northern-Hemisphere winter, *Mon. Wea. Rev.*, *109*, 784–812 .

Wang, C., S.-K. Lee, and D.B. Enfield (2008), Atlantic Warm Pool acting as a link between Atlantic Multidecadal Oscillation and Atlantic tropical cyclone activity, *Geochem. Geophys. Geosyst.*, *9*, Q05V03, doi:10.1029/2007GC001809.

Wang, G., P. Yang, X. Zhou, K. L. Swanson, and A. A. Tsonis (2012), Directional influences on global temperature prediction, Geophys. Res. Lett., 39, L13704, doi:10.1029/2012GL052149.

Weare, B., A. Navato, and R.E. Newell (1976) Empirical orthogonal analysis of Pacific Ocean sea surface temperature. *J. Phys. Oceanogr., 6*, 671–678.

Wyatt, M.G., S. Kravtsov, and A.A. Tsonis, Atlantic multidecadal oscillation and northern hemisphere's climate variability. Clim. Dyn. doi:10.1007/s00382-011-1071-8, 2011

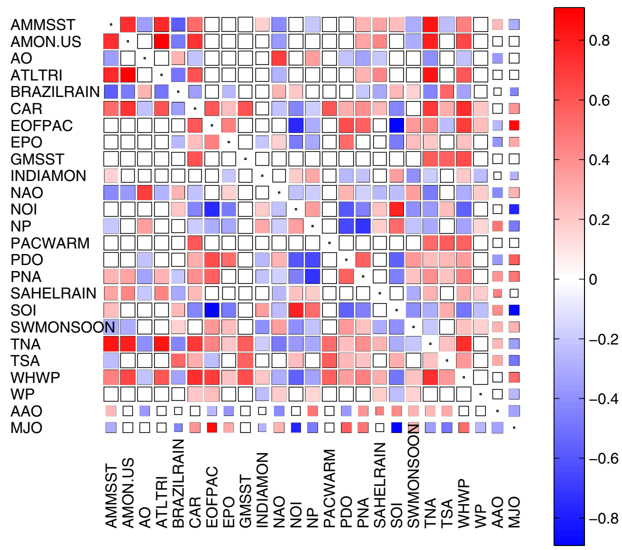

Figure 1. Cross-correlation map between pairs of indices. The size of each square is proportional to the length of the common time interval of availability; the square showing the correlation between two time series with a common interval of 20 years will be twice larger than that showing the correlation between two time series with a common interval of 10 years. Only correlations that are significant at the 95% lever are colored: red means the correlation is positive, blue indicates anti-correlation, while white squares indicate correlations that are not significant at this level. The results for each pair appear twice, for better legibility.

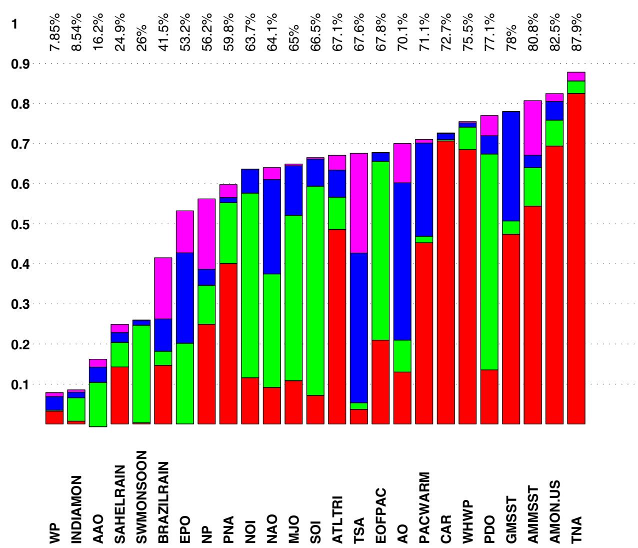

Figure 2. Variance captured by each of the four leading PCs for each of our 25 climate indices, sorted from the least "explained" to the best "explained" index, i.e., from the one that is most independent of the other 24 to the one that is least so. The height of the color bars indicates the variance contribution of the leading PCs, from the first to the fourth: red, green, blue and purple, in this order. The full list of the index acronyms on the abscissa is given in Table 1.

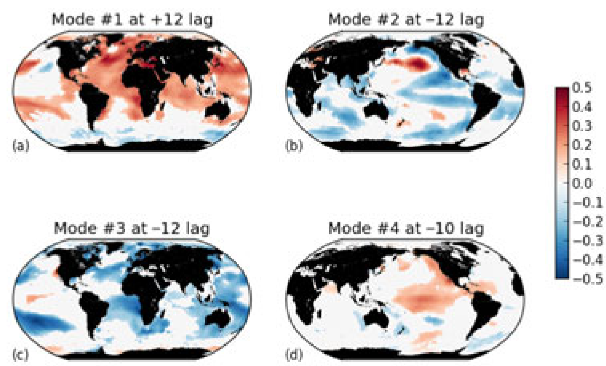

3

Figure 3. Lagged cross-covariances between the local SST (in $^{\circ}C$) and each of the four leading PCs, plotted for the lag that yields the highest sum of absolute values of the cross-correlations: (a)–(d) Modes 1–4, each at the respective optimal lag. Color bar gives the cross-covariance values; zero values (in white) include all cross-correlations that are not significant at the 95% level. Note that, as the PCs are normalized to unit standard deviation, the cross-covariance at a grid point only depends on the standard deviation of the SST there, projected onto the given PC. To better show the most significant areas for each mode, the maps are centered on the Greenwich meridian in panels (a) and (c), while being centered on the dateline in (b) and (d).

Table 1. Climate indices used in this study; for each index, we list its name, time range, optimal set of lags with respect to the Atlantic Meridional Mode index (both unweighted and weighted), and internet adress for the source of the data; ESRL stands for http://www.esrl.noaa.gov/psd/data/correlation

Abbreviation	Index name	Starts	Ends	unweighted lag (months)	weighted lag (months)	Address
AAO	Antarctic Oscillation	1979	2011	-3.5	-4.4	ESRL/aao.data
AMMSST	Atlantic Meridional Mode	1948	2011	0.0	0.0	ESRL/ammsst.data
AMON	Atlantic Multidecadal Oscillation	1948	2011	-0.4	-0.6	ESRL/amon.us.data
AO	Arctic Oscillation	1980	2011	-5.2	-4.8	ESRL/ao.data
ATLTRI	Atlantic Tripole SST EOF	1948	2009	-1.7	-5.6	ESRL/atltri.data
BRAZILRAIN	Northeast Brazil Rainfall Anomaly	1948	2000	5.3	9.4	ESRL/brazilrain.data
CAR	Caribbean SST	1951	2011	-0.3	-0.8	ESRL/CAR.data
EOFPAC	Tropical Pacific SST EOF	1948	2008	1.0	1.1	ESRL/eofpac.data
EPO	East/North Pacific Oscillation	1950	2011	4.0	3.5	ESRL/epo.data
GMSST	Global Mean Land/Ocean Temperature	1948	2011	2.3	3.2	ESRL/gmsst.data
INDIAMON	Central Indian Precipitation	1948	2000	-1.3	0.8	ESRL/indiamon.data
MJO	Madden-Julian Oscillation	1978	2011	-3.5	-4.4	http://climexp.knmi.nl/
NAO	North Atlantic Oscillation	1950	2011	-4.5	-4.6	ESRL/nao.data
NOI	Northern Oscillation	1948	2007	1.0	1.0	ESRL/noi.data
NP	North Pacific pattern	1948	2011	-1.8	-3.6	ESRL/np.data
PACWARM	Pacific Warmpool	1948	2009	3.9	4.1	ESRL/pacwarm.data
PDO	Pacific Decadal Oscillation	1948	2011	1.8	1.9	ESRL/pdo.data
PNA	Pacific North American	1950	2011	1.1	1.8	ESRL/pna.data
SAHELRAIN	Sahel Standardized Rainfall	1948	2001	-4.1	3.4	ESRL/sahelrain.data
SOI	Southern Oscillation	1951	2011	1.4	1.6	ESRL/soi.data
SWMONSOON	SW Monsoon Region rainfall	1948	2011	0.5	1.7	ESRL/swmonsoon.data
TNA	Tropical Northern Atlantic	1948	2011	0.3	0.5	ESRL/tna.data
TSA	Tropical Southern Atlantic	1948	2011	2.7	1.2	ESRL/tsa.data
WHWP	Western Hemisphere warm pool	1948	2011	1.7	1.8	ESRL/whwp.data
WP	Western Pacific Index	1950	2011	-2.3	-0.6	ESRL/wp.data

Table 2. Main periods (in years) of the four leading PCs and their significance level from spectral-density estimates using the multi-taper method (MTM) and the maximum-entropy method (MEM). Note that singular spectrum analysis (SSA) has been used as a pre-filter for the MEM spectrum. Only the periods found for the total reconstruction are given here, and not the ones on the individual SSA modes. All the MTM results are significant at the 99% level according to the robustness test of *Mann and Lees* [1996]; please see text (Section 5) for the SSA+MEM tests.

PC #	SSA+MEM	MTM
1	> 20	
		3.55
	2.84	2.75
	2.03	2.44
2	> 20	
	4.74	4.26
		3.28
	2.51	2.51
3	> 20	
	5.33	5.69
		4.26
		3.45
	2.24	2.31
4	21.3	
		3.28
	2.37	2.50